Article

A Nickel Phosphine Complex as a Fast and Efficient Hydrogen Production Catalyst

Lu Gan, Thomas L. Groy, Pilarisetty Tarakeshwar, Shobeir K.S. Mazinani, Jason Shearer, Vladimiro Mujica, and Anne K. Jones

A Nickel Phosphine Complex as a Fast and Efficient Hydrogen Production Catalyst

Lu Gan[†], Thomas L. Groy[†], Pilarisetty Tarakeshwar[†], Shobeir K. S. Mazinani[†], Jason Shearer[§], Vladimiro Mujica[†], Anne K. Jones[†]*

[†]Department of Chemistry and Biochemistry, Arizona State University, Tempe, AZ

85287, USA

[§]Department of Chemistry, University of Nevada, Reno, Nevada 89557, USA

*To whom correspondence should be addressed

e-mail: jonesak@asu.edu

Tel: 480-965-0356

Abstract:

Here we report the electrocatalytic reduction of protons to hydrogen by a novel S_2P_2 coordinated nickel complex, [Ni(bdt)(dppf)] (bdt=1,2-benzenedithiolate, dppf= 1,1'-bis(diphenylphosphino)ferrocene). The catalysis is fast and efficient with a turnover frequency of 1240 s^{-1} and an overpotential of only 265 mV for half activity at low acid concentrations. Furthermore, catalysis is possible using a weak acid, and the complex is stable for at least four hours in acidic solution. Calculations of the system carried out at the density functional level of theory (DFT) are consistent with a mechanism for catalysis in which both protonations take place at the nickel center.

Introduction

The primary challenge to widespread production of hydrogen for renewable energy applications is to develop efficient catalysts for proton reduction using abundant metals. In this arena, hydrogenases, the biological catalysts for reduction of protons to hydrogen, are without parallel in terms of efficiency. They operate reversibly in weakly acidic, aqueous solutions at turnover frequencies in excess of $1000 \, s^{-1}$ with very low overpotentials.[1,2] Their activity is all the more remarkable considering that they employ only the first row transition metals iron and nickel to catalyze this multi-electron redox transformation.[3,4]

Although a number of heterogeneous inorganic materials including nickel-based nanomaterial are hydrogen production catalysts,[5-11] molecular catalysts offer significant advantages in terms of ease of modification to tune catalysis and amenability to mechanistic and structural characterization.[12] A number of bimetallic, structural model complexes of both [FeFe] and [NiFe]-hydrogenases have been described. In particular, the $Fe_2(\mu\text{-}SR)_2(CO)_4(L)_2$ family of compounds, in which L can be any one of a number of ligands including phosphines, CN^-, and N-heterocyclic carbenes, has provided invaluable structural and functional models of [FeFe]-hydrogenases.[13] On the other hand, although close structural mimics of [NiFe]-hydrogenases have been reported that include such features as tetrathiolate coordination of nickel, strongly π-accepting ligands to the iron, and bridging sulfur coordination,[14-19] only a limited number of functional [NiFe]-models have been described.[20-23]

The most catalytically active proton reduction compounds have not been biomimetic, bimetallic complexes but instead a variety of bio-inspired mononuclear complexes

including Ni and Co phosphines, Co diglyoximes, Co diimine-dioximes, and polypyridyl Co complexes.[24-29] These successful catalysts have suggested bio-inspired design elements that may be useful or even essential in effective hydrogen evolution catalysts based on first row transition metals. For example, DuBois and coworkers, have employed internal proton relays in the second coordination sphere of Ni phosphine complexes to create extraordinarily fast catalysts.[24,30] Other groups have explored the use of redox noninnocent ligands such as 1,2-benzenedithiolate (bdt) as an internal redox buffer to provide the reducing equivalents necessary for the two-electron reaction.[31,32] For example, Ott and coworkers have prepared a series of coordinatively unsaturated, mononuclear Fe complexes supported by bdt, a chelating phosphine, and a single CO ligand that have proven, in some cases, to produce hydrogen from weak acids at high rates and low overpotentials.[33-35] We have also shown that the sterically restrictive ligand 1,1'-bis(diphenylphosphino)ferrocene (dppf) can be used to generate a bio-inspired, coordinatively unsaturated iron complex of unusual geometry that performs hydrogen evolution catalysis with very low overpotentials.[36]

Herein we combine several of these design ideas to create a nickel complex capable of fast reduction of protons from weak acid in THF at unexpectedly low overpotentials. The nickel center features a mixed thiolate/phosphine first coordination sphere coordinated by both the potentially redox active bdt moiety and the sterically demanding dppf ligand. In addition to the possible redox activity of bdt, the thiolate sulfurs of the ligand can, in principle, serve as internal proton transfer conduits, as hypothesized for the cysteine ligands of [NiFe]-hydrogenases. We employ a combination of spectroscopic, and

electrochemical methods to characterize this compound. Based on high-level theoretical calculations, we also propose a reaction mechanism to explain its high catalytic activity.

Results and Discussion

Synthesis and Characterization of [Ni(bdt)(dppf)], 1. The complex [Ni(bdt)(dppf)] (bdt=1,2-benzenedithiolate, dppf= 1, 1'-bis(diphenylphosphino)ferrocene) (**1**) was synthesized in 45 % yield in two steps (Scheme 1). First, 1,1'-bis(diphenylphosphino)ferrocene was mixed with bis(triphenylphosphine) nickel(II) dichloride. The compound (dppf)NiCl$_2$ is likely generated in this step, but attempts were not made to purify it. In a second step, the 1,2-benzenedithiolate was introduced in the presence of sodium methoxide (NaOMe). Purification via silica chromatography yielded the desired, brown, air-stable product.

The molecular structure of **1**, shown in Figure 1, was determined by single crystal X-ray diffraction (statistics shown in Supplementary Table S4). Selected distances and angles are shown in Supplementary Tables S5 and S6. The nickel is in a square planar coordination environment with the iron center within 4.257 Å, and Ni-S and Ni-P distances well within the range expected for square planar nickel complexes. The dppf ligand is known to be sterically demanding,[37] and the most notable structural parameter of **1** is the P-Ni-P angle of 101°. For comparison, the P-Ni-P angle of the closely related [Ni(bdt)(dppe)] (dppe=1,2-bis(diphenylphosphino)ethane) (**2**), which includes a less restrictive chelating phosphine, was reported to be only 86°.[38] As shown in Figure S11, Nickel K-edge X-ray absorption spectra obtained from a frozen solution (THF) are

consistent with the crystallographic formulation of **1**. A prominent pre-edge peak at 8336.4(1) eV is observed in the XANES region of the Ni K-edge X-ray absorption spectrum. This corresponds to the $Ni(1s \rightarrow 4p_z)$ transition and is a characteristic feature contained in the XANES region of the X-ray absorption spectrum for square-planar Ni(II) complexes.[39] The EXAFS region is most consistent with nickel ligated in a P_2S_2 ligand environment with two NiS donors at 2.16 Å and two NiP donors at 2.27 Å. In addition, a well ordered Ni-Fe vector can be located at 4.2 Å. Thus, **1** does not appear to adopt a different geometry in THF solutions relative to the crystal structure.

The electronic properties of **1** were characterized via both NMR and UV-Vis spectroscopy. The UV-vis spectrum (Figure S1) includes the expected features associated with the π-π* transitions of both the ferrocene and the bdt moieties, as well as metal-to-ligand charge transfer bands from nickel to phosphorus and nickel to sulfur. These results, taken together with the NMR spectra and XAS data, can leave little doubt that the solution structure of the complex is similar to that found in the crystal. It is interesting to note that the ^{1}H chemical shifts for the cyclopentadienyl protons of **1** were shifted downfield (δ 4.37 and 4.22 ppm) relative to those of dppf (δ 4.24 and 3.95 ppm). This can be taken as evidence that coordination of the nickel by the phosphines has a measurable impact on the electron density of the nearby cyclopentadienyl rings.

Redox chemistry of 1. Cyclic voltammograms of **1** under argon in THF feature two sets of peaks (Figure 2). The first, a reversible reduction at $E_{1/2}$= -1.280 V (all potentials are quoted relative to SCE; note that the reduction potential of $Fc^{+/0}$ is 0.532 V vs. SCE in THF) can be attributed to the Ni^{II}/Ni^{I} couple. Notably, under continuous potential cycling around the Ni^{II}/Ni^{I} couple in air, no signs of decomposition of the

complex were observed even after 30 minutes. The second feature in the voltammogram is a partially reversible oxidation peak at E_{pa}= +0.744 V, likely corresponding to oxidation of the ferrocenyl iron from Fe(II) to Fe(III). As observed for other dppf complexes, this oxidation causes partial decomposition of the ferrocene phosphine leading to a largely irreversible reaction.[40,41]

By comparison, the CV of **2** features only one set of reversible peaks at -0.518 V corresponding to the Ni^{II}/Ni^{I} couple. We note that the Ni^{II}/Ni^{I} reduction potentials of these two closely related complexes differ by more than 0.75 V, with the reduced form of **2** considerably more stable than that of **1**. Although it is possible that the dppf is a stronger donor, destabilizing the reduced form of **1**, the difference in reduction potentials is larger than might be expected based only on the donor abilities of the ligands. Calculations carried out on both complexes **1** and **2** suggest that changes in the electronic characteristics of their lowest unoccupied molecular orbitals (LUMOs) explain the observed experimental differences (*vide infra*).

Electrocatalytic hydrogen production by 1. Figure 3 shows that addition of the weak acid acetic acid (pKa^{THF}= 22.48)[42] to an electrochemical experiment in the presence of **1** results in an increase of the cathodic current at the potential of the Ni^{II} reduction and disappearance of the corresponding oxidation peak. The more oxidizing couple remains unchanged. This enhancement of current in a single direction is characteristic of electrocatalysis, in this case the reduction of protons to hydrogen. Analysis of the headspace via gas chromatography following controlled potential electrolysis confirmed that hydrogen was produced, and the Faradaic efficiency exceeded 99%. Under identical experimental conditions but in the absence of **1**, negligible reduction of protons by the

glassy carbon working electrode was observed at these potentials, indicating that the catalysis depends on the presence of the NiFe complex. Surprisingly, **2** demonstrated no electrocatalytic activity in the presence of either acetic acid or the considerably stronger acid *p*-toluenesulfonic acid (*p*TsOH).

To ensure that the electrocatalysis was initiated by a molecular species in solution and not by formation of an ill-defined nanoparticulate material at the electrode surface as described by Fang and coworkers,[43] immediately following catalytic cyclic voltammetry, the working electrode was transferred to a fresh acidic solution without dissolved catalyst. In this second solution, i.e. one without catalyst present, catalysis was not observed, indicating that the catalytically active species was not confined to the electrode surface. Furthermore, throughout the electrocatalytic experiments, the color of the solution remained unchanged and precipitate was not observed, suggesting that the catalyst is likely relatively stable even under the acidic conditions employed. This result was confirmed analytically. Figure S9 shows that following four hour exposure to 77 equivalents of acetic acid, the UV-vis spectrum of **1** was unchanged. On the other hand, in the presence of *p*-toluenesulfonic acid (*p*TsOH), with a pKa of 8.3 in acetonitrile a much stronger acid,[34] catalysis was also observed. Although the turnover frequency is clearly higher in *p*TsOH than acetic acid, the catalyst decomposed too quickly in the stronger acid for reliable kinetic analysis (Figure S3).[44]

Figure 4 shows the ratio of catalytic current in the presence of acetic acid (i_c) to the peak current for the reduction of **1** in the absence of acid (i_p) as a function of the acid concentration in the experiment. At concentrations of less than 50 equivalents of acetic acid (relative to catalyst), the observed catalytic current increased linearly with acid

concentration. Beyond this acid concentration, no significant increase in catalytic current was observed (Figure S5 shows voltammograms in the acid independent region). This type of behavior is expected when substrate (H^+) concentration is sufficiently high that it is not depleted by the catalytic process during the course of the experiment and some other elementary step becomes rate limiting in the catalytic cycle. Figures S6 and S7 show that the i_c/i_p data are also independent of both catalyst concentration and the potential scan rate of the cyclic voltammogram. Using data in this acid independent regime, the rate constant for hydrogen evolution (k) can be calculated from the expression

$$\frac{i_c}{i_p} = \frac{n}{0.4463} \sqrt{\frac{RTk}{Fv}}$$

in which v is the potential scan rate, n is the number of electrons transferred (two for hydrogen evolution), R is the universal gas constant, T is the temperature, and F is Faraday's constant.[45] The i_c/i_p values of 80 in the acid independent region (for a scan rate of 100 mV s^{-1}) indicate an acid-independent rate constant of 1240 s^{-1}. Repeating this analysis using independent data sets generated using different electrochemical potential scan rates indicates that the TOF is a robust parameter in the range $1220\text{-}1290 \text{ s}^{-1}$.

Although turnover frequencies are important metrics for characterizing electrocatalysts, it is also important to consider the electrochemical overpotential, essentially an activation energy, required to achieve those rates. Following the method of Fourmond and coworkers,[46] the overpotential required to attain half of the overall catalytic current was determined under all experimental conditions evaluated. This value ranges from 265 mV at low acid concentration to 500 mV at high acid concentration

(using $E^{o}_{H+/H2}$= -.440 V (*vs*. Fc^{+}/Fc)) in THF[47], a pK_a of 22.48 for acetic acid in THF,[42] and pK_a of 7.7 for perchloric acid in THF). The combination of high catalytic efficiency and low overpotential for proton reduction indicate that **1** exhibits high energy-conversion efficiencies for H_2 production.

Reaction of 1 with hydrogen gas. Since **1** catalyzes the reduction of H^{+} at relatively low overpotentials, i.e. near the thermodynamically predicted equilibrium, we hypothesized that it may also interact with hydrogen. As shown in Figure 5, exposure of **1** to a THF solution saturated with hydrogen gas (3.3 mM) resulted in a shift of the potential for the Ni$^{II/I}$ reduction of **1** from $E_{1/2}$= -1.280 V under argon to -1.009 V under hydrogen. Simultaneously, there was a noticeable decrease in the reversibility of the process, i.e. in the presence of hydrogen a clear reoxidation wave is not observed. The ratio of i_{ox} to i_{red} decreases from 0.98 in the absence of hydrogen to 0.70 in the presence of hydrogen. Figure S2 shows that the potential of ferrocene under the same experimental conditions is unaffected by the addition of hydrogen. Thus the shift of the reduction potential of **1** is not the result of a change in the potential of the pseudo-reference electrode but results instead from an interaction of 1 with hydrogen. Interestingly, the interaction of **1** with hydrogen is largely reversible. After replacing the hydrogen gas in the experimental solution with argon via sparging, the reduction peak returns to $E_{1/2}$= -1.280 V with only a slight decrease in the oxidative signal, indicating that a small fraction of the initial complex may not have been recovered.

The shift in reduction potential indicates an interaction between complex **1** and hydrogen gas. The large shift in the potential of the Ni$^{II/I}$ couple in the presence of hydrogen implies that the nickel center is substantially easier to reduce with hydrogen

bound, i.e. hydrogen binds more tightly to the reduced, Ni(I) form of the complex. A thermodynamic square scheme can be used to show that the binding constant for binding to the Ni(I) form is approximately 10^5 times larger than that for the Ni(II) form (see SI). This suggests that the hydrogen ligand withdraws appreciable electron density from the nickel center resulting in stabilization of Ni(I). To understand the nature of the interaction between **1** and hydrogen, efforts were made to characterize **1-H₂** spectroscopically. Note that **1** was not chemically reduced; so these efforts only probe the ability to form Ni(II)-H_2, the less stable complex. Using 1 atm of hydrogen, the hydrogen-bound complex was not detectable in ^{1}H NMR spectra, suggesting the Ni(II) species is exceedingly unstable. The computational results presented below confirm this observation.

Since no signs of electrocatalytic hydrogen oxidation were observed, experiments in the presence of both hydrogen and the base triethylamine were also undertaken. Addition of up to 10 mM triethylamine to a 2.3 mM hydrogen-saturated solution of **1** did not result in any observable changes in the electrochemical response suggesting that **1** is still not capable of hydrogen oxidation under these conditions.

Hydrogen and carbon monoxide have marked similarities as ligands, and thus observation of an interaction with H_2 suggests that external CO may also bind **1**. Cyclic voltammetric experiments demonstrate that **1** does indeed interact with CO. As shown in Figure S8, voltammograms from **1** in the presence of CO feature two irreversible reductions. The first occurs at the noticeably less reducing potential of -0.95 V the second at -1.29 V. As observed for the voltammetry in the presence of H_2, the voltammetric changes attributable to interaction of **1** with CO could be partially reversed by removal of the gas from the experiment by sparging with argon. However, following exposure of **1** to

CO, the initial reversibility of the reduction of **1** under argon is never completely restored. Although the potential of the second reduction is complete to that observed for the **[1]$^{0/1-}$** reduction, the complete irreversibility of the signal in the presence of CO suggests that it arises from a different reaction. We hypothesize that the two reductions of **[1-CO]** are the Ni$^{II/I}$ and Ni$^{I/0}$ reductions. The reduced species may decompose leading to the observed irreversibility. There is some support in the literature for this suggestion. Five coordinate Ni(II) carbonyl complexes are relatively rare, but complexes of the formula NiX$_2$(CO)(PR$_3$)$_2$ where X=halides and PR$_3$= PMe$_3$, PEt$_3$, PMe$_2$Ph, PMePh$_2$, PPh$_3$ have been reported.[48] These compounds can be generated by bubbling CO through the tetracoordinate NiX$_2$(PR$_3$) precursors, much like the procedure used in these electrochemical experiments. Furthermore, when PR$_3$ is PPh$_3$, rapid reduction to Ni(0) is observed.

Computational Studies. We carried out electronic structure calculations on **1** and **2** to explain the electrochemical differences in the two complexes (Tables S1). As may be expected, the most notable difference is related to the P-Ni-P fragment. The calculations indicate that the Ni-P bond orders are substantially higher in **2** than in **1**. Thus, compared to **1**, the Ni-P bonds are shorter in **2**. Interestingly, the Ni-S bond lengths are nearly equal in both complexes. While the calculated HOMO energies of both complexes are similar, the LUMO energies of **2** are slightly lower than that of **1**. Since the LUMO energies are directly correlated to the reduction potentials, this suggests that **2** will be more easily reduced than **1**. We note also that the LUMO orbitals in **2** are more extensively delocalized into the phenyl rings than in **1** (Figure S14).

The experimental data indicate that a one or two electron reduction of **1** precedes a rate determining protonation step. We therefore theoretically explored an alternating electrochemical/chemical mechanism (ECEC) consistent with the experimental data (Figure 6). Since the calculated orbital contributions to the frontier orbitals (Tables S3) indicate a negligible contribution from the ferrocene Fe atom, we believe that the reactivity of **1** is entirely dependent on the Ni atom. Thus, **1** is more analogous to mononuclear Ni or Co catalysts than to other [NiFe] complexes with a metal-metal bond.[20,23,26,28,49-52]

In the first step, **1** is reduced to form a d^9 Ni complex (**20**). Compared to **1**, a substantial distortion of the coordination geometry around the Ni atom can be noted in **20** (Table S2). Since there is evidence for protonation of thiolates in [NiFe]-hydrogenases and some model complexes, we hypothesized that **20** can be protonated either on the Ni atom (**31**) or a thiolate sulfur (**32**).[22,53,54] The calculations indicate that protonation on Ni(**31**) is energetically more favorable by 3.6 kcal/mol. Though this energetic difference is not inconsequential, we investigated the energetics of electron attachment to both complexes. Electron attachment to **31** generates the reduced complex **41** that is 5.3 kcal/mol more stable than **42**, the reduced species formed analogously from **32**. This indicates that reduction of the species with the metal protonated, as opposed to the ligand, is energetically preferred. Subsequent attachment of a proton to either of structure **41** or **42** leads to the formation of **50**, wherein the hydrogen molecule has already formed and dissociated from the Ni atom. To ascertain the preferred pathway for attachment of the second proton to **41** or **42**, we identified the transition state by carrying out a synchronous transit-guided quasi-Newton (STQN) calculation using **41** as a starting structure and **50**

as the final structure. In the structure of the transition state, both hydrogens are bound to the Ni atom forming a pseudo-octahedral geometry transition state. In this transition state, the Ni-S distances are 0.1 Å and the Ni-P 0.15 Å longer than in **1**. The dihedral angles of **1** and **50** also differ by more than 40º. This suggests that the tetrahedral distortion of **1** upon reduction is crucial in creating adjacent, accessible open coordination sites for attachment of both protons to the metal and likely key in facilitating fast catalysis. Furthermore, the calculated bond orders indicate that a covalent metal hydride is formed in the course of proposed mechanism.

Conclusion

Although **1** is a bimetallic [NiFe] complex, functionally it can be more accurately thought of as analogous to mononuclear nickel complexes. The structure of the complex suggests the two metals are too far apart from one another for any bonding interaction, and the DFT results confirm this interpretation. Instead, the rigidity and the bite angle of the chelating ddpf ligand are likely its most relevant properties, strictly enforcing square planar geometry on the nickel (II) center and concomitantly tuning both the redox properties and the acidity of the catalytic site. The result is that **1** is a stable and remarkably efficient catalyst with not only a high turnover frequency but also low overpotential.

Energetically efficient proton reduction catalysts that function in water at near neutral pH are necessary to bring electrocatalytic production of hydrogen into an economically appealing regime. The insolubility of **1** in water currently precludes its use in such an application. However, the structure of **1** is eminently suitable to ligand modifications that will facilitate the introduction of functionalities to tune both the

catalytic properties and the solubility. Thus these results should inspire the synthesis and characterization of new compounds that will both provide insight into the mechanisms of hydrogenases and related model complexes and replace precious metal catalysts in hydrogen production/utilization applications.

Materials and Methods

General Methods. Reactions were carried out under an atmosphere of nitrogen using standard Schlenk and high-vacuum techniques. Tetrahydrofuran (THF) and diethyl ether were dried over sodium/benzophenone under nitrogen and freshly distilled prior to use; dichloromethane was dried over calcium hydride under nitrogen and freshly distilled prior to use; methanol was dried over magnesium/iodine under nitrogen and freshly distilled prior to use. All the other chemicals were purchased from Sigma–Aldrich of the highest purity available and used as received without further purification.

Instrumentation. ^{1}H and ^{31}P NMR spectra were recorded at 400 MHz (for ^{1}H) using Varian Liquid-State NMR instruments in deuterated solvents containing 0.1% TMS (tetramethylsilane) unless otherwise mentioned. UV/Vis measurements were performed on a Hewlett–Packard 8453 spectrophotometer using quartz cuvettes with a 1 cm path length. Cyclic voltammetry measurements were performed with an AutoLab model PGSTAT 128N potentiostat/galvanostat electrochemical system with a conventional three-electrode cell at room temperature (298K). The working electrode was a glassy carbon electrode with a 3 mm diameter, the auxiliary electrode consisted of a platinum wire, and a silver wire in the corresponding organic solvent with 0.3 M tetrabutylammonium hexafluorophosphate (TBAPF$_6$) was used as the reference electrode. High purity argon was used to maintain an inert atmosphere during experiments.

Potentials were calibrated by measuring Fc^+/Fc under the same conditions and adjusted to SCE based on the relation E Fc^+/Fc=0.416 V vs. SCE.[55]

Controlled potential electrolysis was performed in a BASi bulk electrolysis cell using a reticulated vitreous carbon (cylinder 55 mm length, 40 mm diameter, and 5 mm deep) working electrode. The reference electrode was placed in a separate compartment and electrical connectivity maintained via a fine porosity glass frit. Dearation of solutions was achieved by bubbling argon for 15 minutes, and the electrochemical cell was then sealed to allow headspace analysis. Gas withdrawals from the headspace were made with a Hamilton 1750 SL locking gas-tight syringe and were compensated with an equal addition of argon. A Varian CP-3800 gas chromatograph (thermal conductivity detector, Alltech Porapak Q 80/100 column, Argon as carrier gas) was used to determine the hydrogen concentration following calibration with known concentrations of H_2 over the region 0-3.0 %.

Single crystal X-ray diffraction. The crystal was mounted on the end of a thin glass fiber using Apiezon type N grease and optically centered. Cell parameter measurements and single-crystal diffraction data collection were performed at low temperature (123 K) with a Bruker Smart APEX diffractometer using graphite monochromated Mo Kα radiation (λ = 0.71073 Å) in the ω−φ scanning mode. The structure was solved by direct methods and refined by full-matrix least-squares on F^2. The following is the list of the programs used: data collection, Bruker Instrument Service v2010.9.0.0; cell refinement and data reduction, SAINT V7.68A; absorption correction, SADABS 2008/1; structure solution and refinement, SHELXS-97; molecular graphics, XShell v6.3.1; preparation of material for publication, Bruker APEX2 v2010.9-1.[56-60]

Details of crystal data and parameters for data collection and refinement are listed in Table S3.

Nickel K-edge X-ray Absorption Spectroscopy. [Ni(bdt)(dppf)] was dissolved in THF to a final concentration of 2.0 mM. The solution was then injected into aluminum sample holders with Kapton tape windows and frozen in liquid nitrogen. All data were collected on beamline X3b at the National Synchrotron Light Source (NSLS, Brookhaven National Laboratories, Upton, NY). Samples were maintained at ~25 K using a helium displex cryostat throughout data collection, and all data were obtained as fluorescence data using a 31 element solid-state Ge detector with a 3 micron Co metal filter between the sample chamber and the detector. Total count rates were maintained under 50 kHz. Data were collected in 5 eV steps from 8133 – 8313 eV (1 second integration time per point), 0.3 eV steps from 8313 – 8363 eV (3 second integration time per point), 2 eV steps from 8363 – 8633 eV (5 second integration time per point), and 5 eV steps from 8633 eV – 16 k (5 second integration time per point). Individual data sets were inspected prior to data averaging and each spectrum represents the averaged sum of 5 data sets. Data analysis and work-up were performed using EXAFS123 as previously described.[61] Refinements are based on unfiltered $k^3(\chi)$ data refined over the range of $k = 2 - 15$ Å.

Synthesis of [Ni(bdt)(dppf)], 1. 1,1'-Bis(diphenylphosphino)ferrocene (0.1663 g, 0.3000 mmol) was dissolved in 15 ml freshly distilled THF resulting in a yellow solution. Upon addition of 10 ml bis(triphenylphosphine)nickel(II) dichloride in methanol (0.1962 g, 0.2999 mmol), the reaction mixture turned orange. The reaction mixture was then stirred at room temperature for 5 h, after which time the solvent was removed under a vacuum resulting in a bright yellow solid. Dissolving the solid in dichloromethane

(10 ml) yielded a dark green solution. The solution was treated with 1,2-benzenedithiol (34.6 μL, 0.301 mmol) followed by dropwise addition of a sodium methoxide/ methanol solution (14.2 mg sodium, 0.617 mmol, in 3 ml MeOH). The resulting brown solution was stirred for 30 minutes before the solvent was removed under vacuum. The crude compound was purified over a silica column (2.5 cm i.d.) using 2:1 ethyl acetate: dichloromethane. The first yellow band was eluted and fractions dried under a vacuum. The compound was then purified on a second silica column using 3:1:1 hexanes: dichloromethane: ethyl acetate as eluent. The second band eluting from that column was dried under a vacuum to yield the brown **1**, (0.1025 g, 45 % yield). X-ray quality crystals of **1** were grown by layering diethyl ether over a saturated dichloromethane solution and storing in a -20 C freezer in air. ^{1}H NMR (400 MHz, CD$_2$Cl$_2$): δ 7.89 ppm (8 H, m, aromatic on phenyl), 7.49 ppm (4 H, t, aromatic on phenyl), 7.38 ppm (8 H, t, aromatic on phenyl), 7.10 ppm (2 H, dd, aromatic of bdt), 6.74 ppm (2 H, dd, aromatic of bdt), 4.37 ppm (4 H, s, Cp), and 4.22 ppm (4 H, s, Cp); ^{31}P NMR (400 MHz, CD$_2$Cl$_2$): δ 26.9 ppm; UV-vis: λ_{max} 229 nm (ε=91,690 M^{-1} cm^{-1}), λ_{max} 269 nm (ε=57,990 M^{-1} cm^{-1}), λ_{max} 312 nm (ε=38,430 M^{-1} cm^{-1}) and λ_{max} 410 nm (ε=1,288 M^{-1} cm^{-1}). Anal. Calcd for C$_{40}$H$_{32}$FeNiP$_2$S$_2$ (found): C, 63.777(63.788); H, 4.282(4.997).

Synthesis of [Ni(bdt)(dppe)], 2. A 20 ml red clear dichloromethane solution of [1,2-bis(diphenylphosphino)ethane]dichloronickel(II) (0.1382 g, 0.2617 mmol) was treated with 1,2-benzenedithiol (30.1 μL, 0.2616 mmol) followed by dropwise addition of a sodium methoxide/ methanol solution (12.6 mg sodium, 0.548 mmol, in 2.5 ml MeOH). The resulting red solution was stirred for 30 minutes before solvent was

removed under vacuum. The crude compound was recrystallized from dichloromethane/ hexanes to yield a red crystalline solid (0.1285 g, 82 % yield). ^{1}H NMR (400 MHz, CDCl$_3$): δ 7.81 ppm (8 H, m, aromatic on phenyl), 7.45 ppm (12 H, t, aromatic on phenyl), 7.38 ppm (2 H, dd, aromatic of bdt), 6.80 ppm (2 H, dd, aromatic of bdt), and 2.35 ppm (4 H, d, ethane). ^{31}P NMR (400 MHz, CDCl$_3$): δ 58.28 ppm. Anal. Calcd for C$_{32}$H$_{28}$NiP$_2$S$_2$ (found): C, 64.353(64.156); H, 4.692(4.884).

Computational Details. Density functional theory (DFT) calculations were carried out using the Becke gradient-corrected exchange functional and Lee−Yang−Parr correlation functional with three parameters (B3LYP) and the 6-31G* basis set using the ORCA and Gaussian suites of programs.[62-71] Since some of these complexes are open-shell systems, calculations were also carried out at the BP86/def2-TZVP level.[72] Scalar relativistic effects were introduced using the zero order regular approximation (ZORA).[73,74] Calculations at this level of theory have been found to yield energies and spectroscopic parameters comparable to those obtained with higher levels of theory and larger basis sets.[75-77] The synchronous transit-guided quasi-Newton (STQN) method was employed to identify the transition state.[78]

Supporting Information Available: Crystallographic data, UV-vis spectra, NMR spectra, additional electrochemical data, thermodynamic calculation, summary of geometrical parameters, Mayer's bond orders, HOMO/LUMO energies and orbital contributions determined by DFT, complete references 28 and 69. This material is available free of charge via the Internet at http://pubs.acs.org.

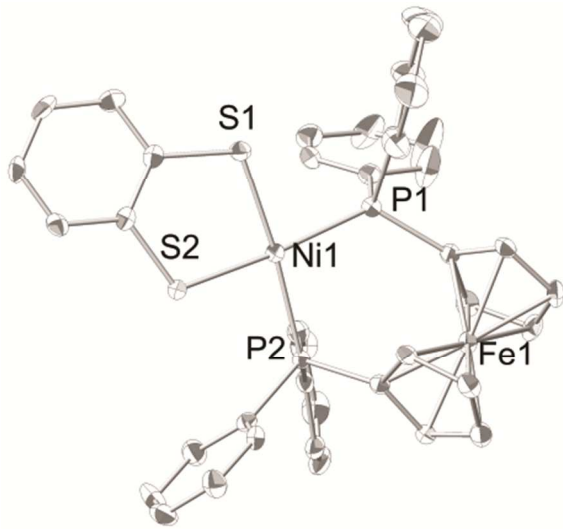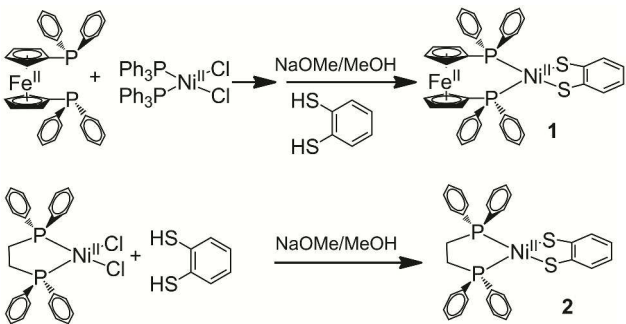**Scheme 1:** Summary of synthetic procedures.

Figure 1. Molecular crystal structure of **1**. Solvent and protons have been deleted for clarity. Thermal elipsoids are shown at 50 % probability.
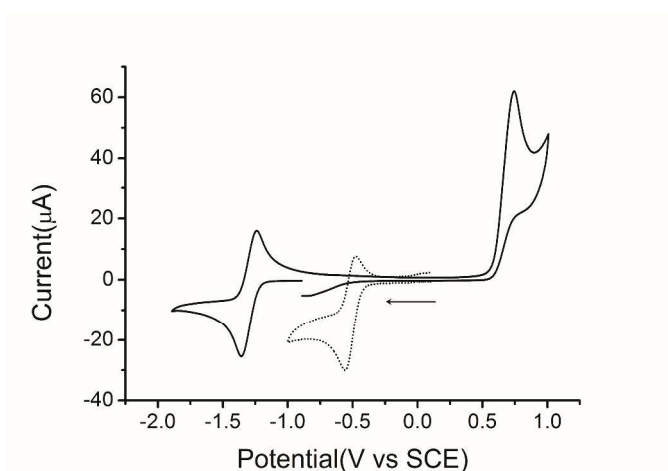
Figure 2: Cyclic voltammograms of **1** (solid line, 3 mM in THF) and **2** (dotted line, 2.7 mM) in THF at a potential scan rate of 100 mV s^{-1}. The supporting electrolyte is 0.3 M TBAPF$_6$. The arrow indicates the starting point and direction of potential cycling.
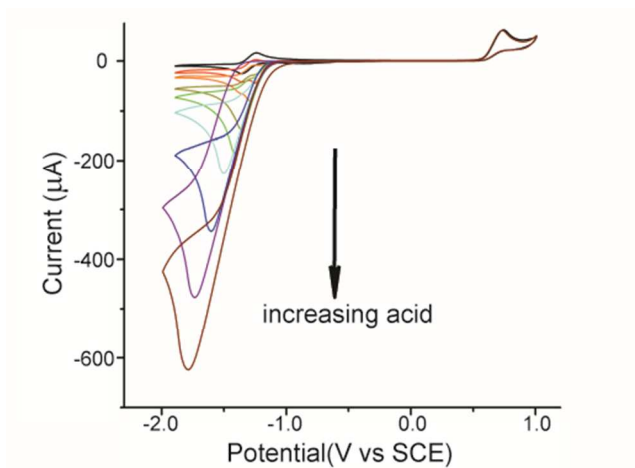

Figure 3. Cyclic voltammograms of **1** in the presence of varying concentrations of CH$_3$CO$_2$H. The experimental conditions are 2.6 mM **1** in THF, 0.3 M TBAPF$_6$, and an electrochemical potential scan rate of 100 mV s^{-1}. The CH$_3$CO$_2$H concentrations are 0, 6.0, 8.0, 12.0, 16.0, 20.0, 30.0, 40.0, and 50.0 mM.
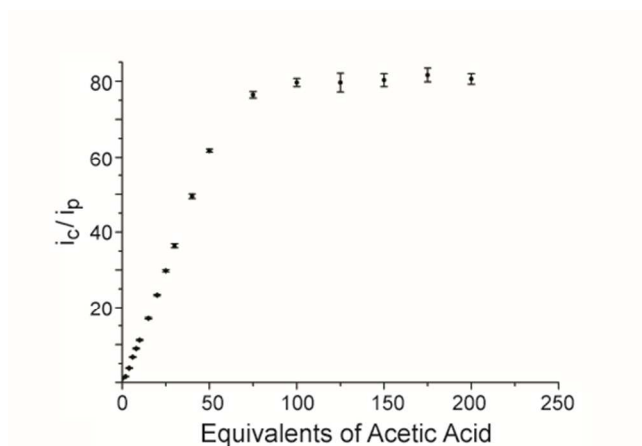
Figure 4. Dependence of normalized catalytic current, i_c, on concentration of CH_3COOH. Currents were extracted from voltammograms such as those shown in Figure 3 that were collected under the following experimental conditions: 2.0 mM **1** in THF, 0.3 M TBAPF$_6$ and an electrochemical potential scan rate of 100 mV s^{-1}. Error bars indicate the standard deviation calculated from three independent measurements.
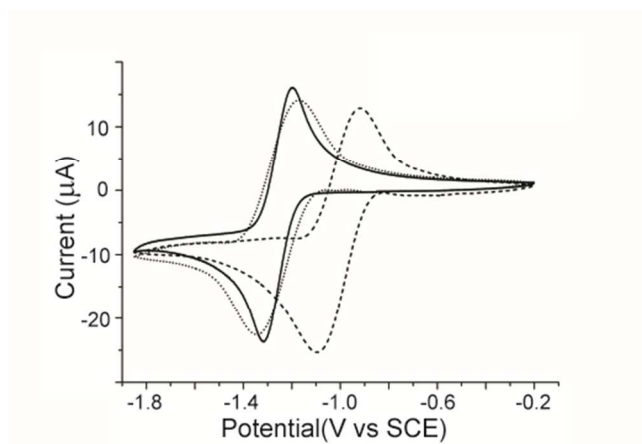

Figure 5. Cyclic voltammograms of **1** in the presence and absence of hydrogen. The solid line shows the voltammogram before exposure of the solution to hydrogen. The dash line shows the voltammograms in a solution saturated with 1 atm hydrogen prepared by sparging immediately preceding measurement. The dotted line shows the voltammogram

after the hydrogen was replaced by sparging the experimental solution with argon. The

experimental conditions are 2.6 mM **1** in THF, 0.3 M TBAPF$_6$, and an electrochemical
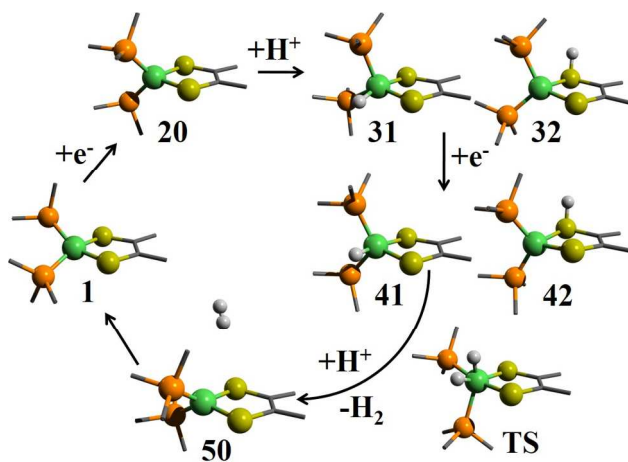
potential scan rate of 100 mV s^{-1}.

Figure 6. Proposed mechanistic scheme (based on optimized structures) for H$_2$

production by **1**. Green balls represent a nickel ion, orange represent phosphorous and

yellow represents sulfur.

References

(1)   Jones, A. K.; Sillery, E.; Albracht, S. P. J.; Armstrong, F. A. *Chem. Commun.* **2002**, 866.

(2)   Madden, C.; Vaughn, M. D.; Diez-Perez, I.; Brown, K. A.; King, P. W.; Gust, D.; Moore, A. L.; Moore, T. A. *J. Am. Chem. Soc.* **2012**, *134*, 1577.

(3)   Armstrong, F. A. *Curr. Opin. Chem. Biol.* **2004**, *8*, 133.

(4)   Fontecilla-Camps, J. C.; Volbeda, A.; Cavazza, C.; Nicolet, Y. *Chem. Rev.* **2007**, *107*, 4273.

(5)   Popczun, E. J.; McKone, J. R.; Read, C. G.; Biacchi, A. J.; Wiltrout, A. M.; Lewis, N. S.; Schaak, R. E. *J. Am. Chem. Soc.* **2013**, *135*, 9267.

(6)   Jaramillo, T. F.; Jorgensen, K. P.; Bonde, J.; Nielsen, J. H.; Horch, S.; Chorkendorff, I. *Science* **2007**, *317*, 100.

(7)   Gu, S.; Du, H. F.; Asiri, A. M.; Sun, X. P.; Li, C. M. *Phys. Chem. Chem. Phys.* **2014**, *16*, 16909.

(8)   Lukowski, M. A.; Daniel, A. S.; English, C. R.; Meng, F.; Forticaux, A.; Hamers, R. J.; Jin, S. *Energ. Environ. Sci.* **2014**, *7*, 2608.

(9)   He, C. Y.; Wu, X. L.; He, Z. Q. *J. Phys. Chem. C* **2014**, *118*, 4578.

(10)   Sun, Y. J.; Liu, C.; Grauer, D. C.; Yano, J. K.; Long, J. R.; Yang, P. D.; Chang, C. J. *J. Am. Chem. Soc.* **2013**, *135*, 17699.

(11)   Chen, W. F.; Sasaki, K.; Ma, C.; Frenkel, A. I.; Marinkovic, N.; Muckerman, J. T.; Zhu, Y. M.; Adzic, R. R. *Angew. Chem.* **2012**, *51*, 6131.

(12)   Artero, V.; Fontecave, M. *Chem. Soc. Rev.* **2013**, *42*, 2338.

(13)   Tard, C.; Pickett, C. J. *Chem. Rev.* **2009**, *109*, 2245.

(14) Perra, A.; Davies, E. S.; Hyde, J. R.; Wang, Q.; McMaster, J.; Schroder, M. *Chem. Commun.* **2006**, 1103.

(15) Li, Z.; Ohki, Y.; Tatsumi, K. *J. Am. Chem. Soc.* **2005**, *127*, 8950.

(16) Tanino, S.; Li, Z.; Ohki, Y.; Tatsumi, K. *Inorg. Chem.* **2009**, *48*, 2358.

(17) Jiang, J.; Maruani, M.; Solaimanzadeh, J.; Lo, W.; Koch, S. A.; Millar, M. *Inorg. Chem.* **2009**, *48*, 6359.

(18) Ohki, Y.; Yasumura, K.; Kuge, K.; Tanino, S.; Ando, M.; Li, Z.; Tatsumi, K. *Proc. Natl. Acad. Sci. USA* **2008**, *105*, 7652.

(19) Ohki, Y.; Tatsumi, K. *Eur. J. Inorg. Chem.* **2011**, 973.

(20) Barton, B. E.; Whaley, C. M.; Rauchfuss, T. B.; Gray, D. L. *J. Am. Chem. Soc.* **2009**, *131*, 6942.

(21) Canaguier, S.; Field, M.; Oudart, Y.; Pecaut, J.; Fontecave, M.; Artero, V. *Chem. Commun.* **2010**, *46*, 5876.

(22) Weber, K.; Kraemer, T.; Shafaat, H. S.; Weyhermueller, T.; Bill, E.; van Gastel, M.; Neese, F.; Lubitz, W. *J. Am. Chem. Soc.* **2012**, *134*, 20745.

(23) Kaur-Ghumaan, S.; Stein, M. *Dalton T.* **2014**, *43*, 9392.

(24) Helm, M. L.; Stewart, M. P.; Bullock, R. M.; DuBois, M. R.; DuBois, D. L. *Science* **2011**, *333*, 863.

(25) Du, P. W.; Eisenberg, R. *Energ. Environ. Sci.* **2012**, *5*, 6012.

(26) Jacques, P. A.; Artero, V.; Pecaut, J.; Fontecave, M. *Proc. Natl. Acad. Sci. USA* **2009**, *106*, 20627.

(27) Hu, X. L.; Brunschwig, B. S.; Peters, J. C. *J. Am. Chem. Soc.* **2007**, *129*, 8988.

(28) Andreiadis, E. S., et al. *Nat. Chem.* **2013**, *5*, 48.

(29)   Artero, V.; Chavarot-Kerlidou, M.; Fontecave, M. *Angew. Chem. Int. Ed.* **2011**, *50*, 7238.

(30)   Bullock, R. M.; Appel, A. M.; Helm, M. L. *Chem. Commun.* **2014**, *50*, 3125.

(31)   McNamara, W. R.; Han, Z.; Alperin, P. J.; Brennessel, W. W.; Holland, P. L.; Eisenberg, R. *J. Am. Chem. Soc.* **2011**, *133*, 15368.

(32)   McNamara, W. R.; Han, Z.; Yin, C.-J.; Brennessel, W. W.; Holland, P. L.; Eisenberg, R. *Proc. Natl. Acad. Sci. USA* **2012**, *109*, 15594.

(33)   Kaur-Ghumaan, S.; Schwartz, L.; Lomoth, R.; Stein, M.; Ott, S. *Angew. Chem. Int. Edit.* **2010**, *49*, 8033.

(34)   Beyler, M.; Ezzaher, S.; Karnahl, M.; Santoni, M.-P.; Lomoth, R.; Ott, S. *Chem. Commun.* **2011**, *47*, 11662.

(35)   Orthaber, A.; Karnahl, M.; Tschierlei, S.; Streich, D.; Stein, M.; Ott, S. *Dalton Trans.* **2014**, *43*, 4537.

(36)   Roy, S.; Mazinani, S. K. S.; Groy, T. L.; Gan, L.; Tarakeshwar, P.; Mujica, V.; Jones, A. K. *Inorg. Chem.* **2014**, *53*, 8919.

(37)   van Haaren, R. J.; Goubitz, K.; Fraanje, J.; van Strijdonck, G. P. F.; Oevering, H.; Coussens, B.; Reek, J. N. H.; Kamer, P. C. J.; van Leeuwen, P. W. N. M. *Inorg. Chem.* **2001**, *40*, 3363.

(38)   Darkwa, J. *Inorg. Chim. Acta* **1997**, *257*, 137.

(39)   Colpas, G. J.; Maroney, M. J.; Bagyinka, C.; Kumar, M.; Willis, W. S.; Suib, S. L.; Baidya, N.; Mascharak, P. K. *Inorg. Chem.* **1991**, *30*, 920.

(40)   Corain, B.; Longato, B.; Favero, G.; Ajo, D.; Pilloni, G.; Russo, U.; Kreissl, F. R. *Inorg. Chim. Acta* **1989**, *157*, 259.

(41)   Pilloni, G.; Longato, B.; Corain, B. *J. Organometal. Chem.* **1991**, *420*, 57.

(42)   Barron, D.; Buti, S.; Ruiz, M.; Barbosa, J. *Polyhedron* **1999**, *18*, 3281.

(43)   Fang, M.; Engelhard, M. H.; Zhu, Z.; Helm, M. L.; Roberts, J. A. S. *ACS Catalysis* **2014**, *4*, 90.

(44)   Guthrie, J. P. *Canadian Journal of Chemistry-Revue Canadienne De Chimie* **1978**, *56*, 2342.

(45)   Bard, A. J.; Faulkner, L. R. *Electrochemical Methods: Fundamentals and Applications*; 2 ed.; Wiley: New York, 2001.

(46)   Fourmond, V.; Jacques, P.-A.; Fontecave, M.; Artero, V. *Inorg. Chem.* **2010**, *49*, 10338.

(47)   Daniele, S.; Ugo, P.; Mazzocchin, G.-A.; Bontempelli, G. *Anal Chim Acta* **1985**, *173*, 141.

(48)   Saint-Joly, C.; Mari, A.; Gleizes, A.; Dartiguenave, M.; Dartiguenave, Y.; Galy, J. *Inorg. Chem.* **1980**, *19*, 2403.

(49)   Barton, B. E.; Rauchfuss, T. B. *J. Am. Chem. Soc.* **2010**, *132*, 14877.

(50)   DuBois, M. R.; Dubois, D. L. *Accounts Chem. Res.* **2009**, *42*, 1974.

(51)   DuBois, M. R.; DuBois, D. L. *Chem. Soc. Rev.* **2009**, *38*, 62.

(52)   Liu, T. B.; DuBois, D. L.; Bullock, R. M. *Nat. Chem.* **2013**, *5*, 228.

(53)   Wombwell, C.; Reisner, E. *Dalton T.* **2014**, *43*, 4483.

(54)   Lee, C.-M.; Chen, C.-H.; Ke, S.-C.; Lee, G.-H.; Liaw, W.-F. *J. Am. Chem. Soc.* **2004**, *126*, 8406.

(55)   Caravana, C.; Giandomenico, C. M.; Lippard, S. J. *Inorg. Chem.* **1982**, *21*, 1860.

(56)   ; Bruker AXS Inc.: Madison, WI, USA, 2008.

(57)   ; Bruker AXS Inc.: Madison, WI, USA, 2004.

(58)   Sheldrick, G. M. *Acta Cryst. A* **2008**, *64*, 112.

(59)   ; Bruker AXS Inc.: Madison, WI, USA, 2010.

(60)   ; Bruker AXS Inc.: Madison, WI, USA, 2009.

(61)   Neupane, K. P.; Shearer, J. *Inorg. Chem.* **2006**, *45*, 10552.

(62)   Francl, M. M.; Pietro, W. J.; Hehre, W. J.; Binkley, J. S.; Gordon, M. S.; Defrees,

        D. J.; Pople, J. A. *J. Chem. Phys.* **1982**, *77*, 3654.

(63)   Lee, C. T.; Yang, W. T.; Parr, R. G. *Phys. Rev. B* **1988**, *37*, 785.

(64)   Becke, A. D. *J. Chem. Phys.* **1993**, *98*, 5648.

(65)   Stephens, P. J.; Devlin, F. J.; Chabalowski, C. F.; Frisch, M. J. *J. Phys. Chem.*

        1994, *98*, 11623.

(66)   Rassolov, V. A.; Pople, J. A.; Ratner, M. A.; Windus, T. L. *J. Chem. Phys.* **1998**,

        109, 1223.

(67)   Neese, F. *WIREs Comput. Mol. Sci.* **2012**, *2*, 73.

(68)   Harihara, P. C.; Pople, J. A. *Theoret. Chimica Acta* **1973**, *28*, 213.

(69)   Frisch, M. J., et al. *Gaussian 03, Revision C.02*; Gaussian, Inc. : Wallingford, CT,

        2004.

(70)   Liu, Y.-C.; Chu, K.-T.; Jhang, R.-L.; Lee, G.-H.; Chiang, M.-H. *Chem. Commun.*

        2013, *49*, 4743.

(71)   Gorelsky, S. I. AOMix program, http://www.sg-chem.net/.

(72)   Weigend, F.; Ahlrichs, R. *Phys. Chem. Chem. Phys.* **2005**, *7*, 3297.

(73)   van Lenthe, E.; Snijders, J. G.; Baerends, E.-J. *J. Chem. Phys.* **1996**, *105*, 6505.

(74)   van Lenthe, E.; Ehlers, A.; Baerends, E.-J. *J. Chem. Phys.* **1999**, *110*, 8943.

(75)   Delcey, M. G.; Pierloot, K.; Phung, Q. M.; Vancoille, S.; Lindh, R.; Ryde, U.

Phys. Chem. Chem. Phys. **2014**, *16*, 7927.

(76)   Roemelt, M.; Maganas, D.; DeBeer, S.; Neese, F. *J. Chem. Phyx.* **2013**, *138*,

204101.

(77)   Siegbahn, P. E.; Tye, J. W.; Hall, M. B. *Chem. Rev.* **2007**, *107*, 4414.

(78)   Ayala, P. Y.; Schlegel, H. B. *J. Chem. Phys.* **1997**, *107*, 375.

1
2
3
4
5
6
7
8
9
10
11
12
13
14
15
16
17
18
19
20
21
22
23
24
25
26
27
28
29
30
31
32
33
34
35
36
37
38
39
40
41
42
43
44
45
46
47
48
49
50
51
52
53
54
55
56
57
58
59
60

TOC Graphic: